INTEGRATING SOLAR PROCESS HEAT INTO MANGANESE ORE PRE-HEATING

M Lubkoll[1,a), S A C Hockaday[2,b), T M Harms[1,c), T W von Backström[1,d), L Amsbeck[3,e) and R Buck[3,f)

[1] Solar Thermal Energy Research Group (STERG), Dept. Mechanical and Mechatronic Engineering, University of Stellenbosch, South Africa; +27 (0)21 808 4242;
[2] Mintek, Private Bag X3015, Randburg, South Africa;
[3] Institute of Solar Research, German Aerospace Center (DLR), Stuttgart, Germany;

a) Matti@sun.ac.za
b) LinaH@mintek.co.za
c) tmh@sun.ac.za
d) twvb@sun.ac.za
e) Lars.Amsbeck@dlr.de
f) Reiner.Buck@dlr.de

Abstract

Recent technology innovation in the fields of concentrating solar energy is opening new potential markets to be considered for viability. In particular, Stellenbosch University's low-cost, high-performance heliostat technology, HelioPod, in combination with the DLR's centrifugal high-temperature particle receiver, CentRec, can provide process heat to industrial processes at high temperatures, exceeding 600 °C. The minerals processing industry operates numerous processes that require high temperatures, such as sintering plants or smelters providing a potential match.

In South Africa, some mining activities and associated processing occur in regions of high solar irradiation, in particular the Northern Cape. This paper considers the viability of providing process heat on the case study of a Manganese sinter plant situated in the Northern Cape. Currently the required ignition temperature of 600 °C is provided by combusting diesel fuel.

The analysis shows that providing high temperature process heat through concentrating solar thermal (CST) technology can lead to significant cost reduction compared to burning diesel. Further benefits are the reduction in CO_2 emissions resulting in an added premium to the product value as well as potential cost reduction, should CO_2 taxation be implemented in future.

Keywords: CST, high temperature process heat, HelioPod, CentRec, particle receiver, Manganese sintering

1. Introduction

The motivation to investigate concentrating solar thermal (CST) application for the minerals processing industry is two-fold. On the one hand, direct benefits through lower levelized cost of heat (LCOH) compared to current conventional solutions can lead to improved production costs for plants. On the other hand, current minerals processing is emission intensive and therewith in contrast to global initiatives to reduce emissions. A direct additional benefit expected for a process plant which employs CST solutions is the added product value through reduced carbon emissions (e.g. through carbon tax or market demand for carbon lean products).

1.1 Context

The global community attempts to significantly reduce carbon emissions in an effort to curb global warming and the greenhouse effect associated with CO_2 in the atmosphere. The European Commission in targeting reduction in carbon emissions by 80 % to 95 % compared to 1990 values by 2050 [1]. To achieve such goals significant reduction in carbon emissions are required outside the publicly discussed fields of mobility and electricity generation.

This requirement by the European Commission is representative for the needs of the entire developed world where notable emission reductions are required. In this context a separate Horizon2020 project proposal was confirmed in April 2018, in-

Fig. 1: Location of the Kalagadi Manganese sintering plant.

cluding the institutions associated with this paper's authors[1]. That project considers, amongst other activities, the solar pre-heating of manganese ore prior to entering a smelter.

1.2 Plant under consideration

1.2.1 Location

Minerals are typically a commodity for export purposes where a significant share of processing may occur in other countries. Mn can be sintered to increase the Mn content of the ore prior to shipping/transportation. This work presents a case study with the example of the Kalagadi Manganese sintering plant near Hotazel, South Africa. Fig. 1 shows the location of the sinter plant.

The sinter plant is situated in the region of Manganese resources in South Africa. Fig. 2 illustrates several other open pit mines in the direct proximity to the Kalagadi sintering plant.

The excellent solar resource at the location of these mines is of high interest. The highest direct normal irradiation (DNI) levels in South Africa are expected to be just below 3300 kWh/m^2 per year in the Northern Cape province in the region between Springbok and Upington (see Fig. 3). The region of high DNI levels spans over the area of Manganese mining activities. The DNI for Hotazel is expected to be approximately 2750 kWh/(m^2 a).
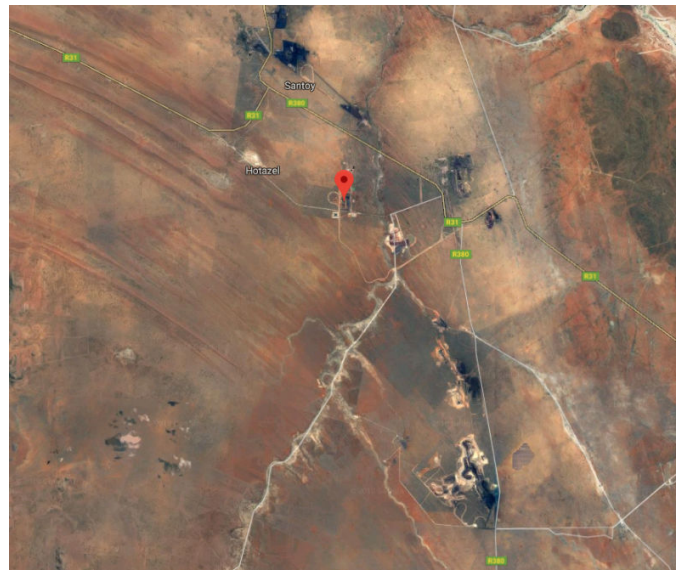

Fig. 2: Satellite image of the Kalagadi Manganese sintering plant and the open pit mines in the proximity. The town of Hotazel is situated to the east of the plant.

This level of solar resource compares favourably to European countries such as Spain where DNI levels below 2200 kWh/(m^2 a) are considered high. It is clear that the high local solar irradiation in the region of mining and minerals processing industry provides potential to be exploited for a global competitive advantage.
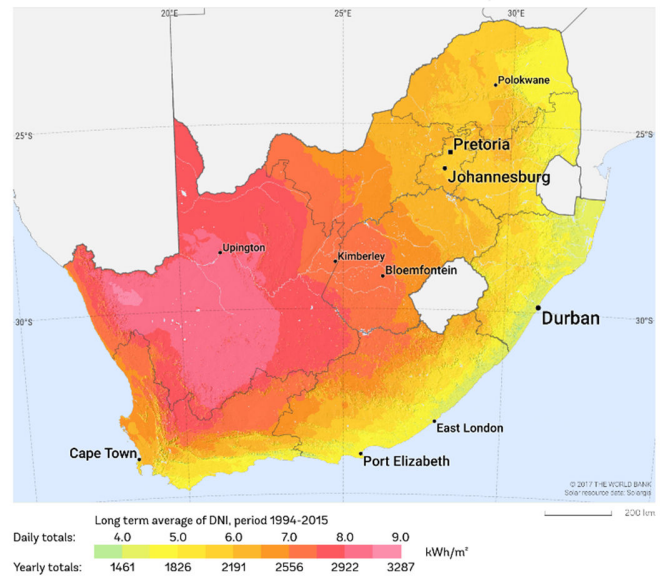
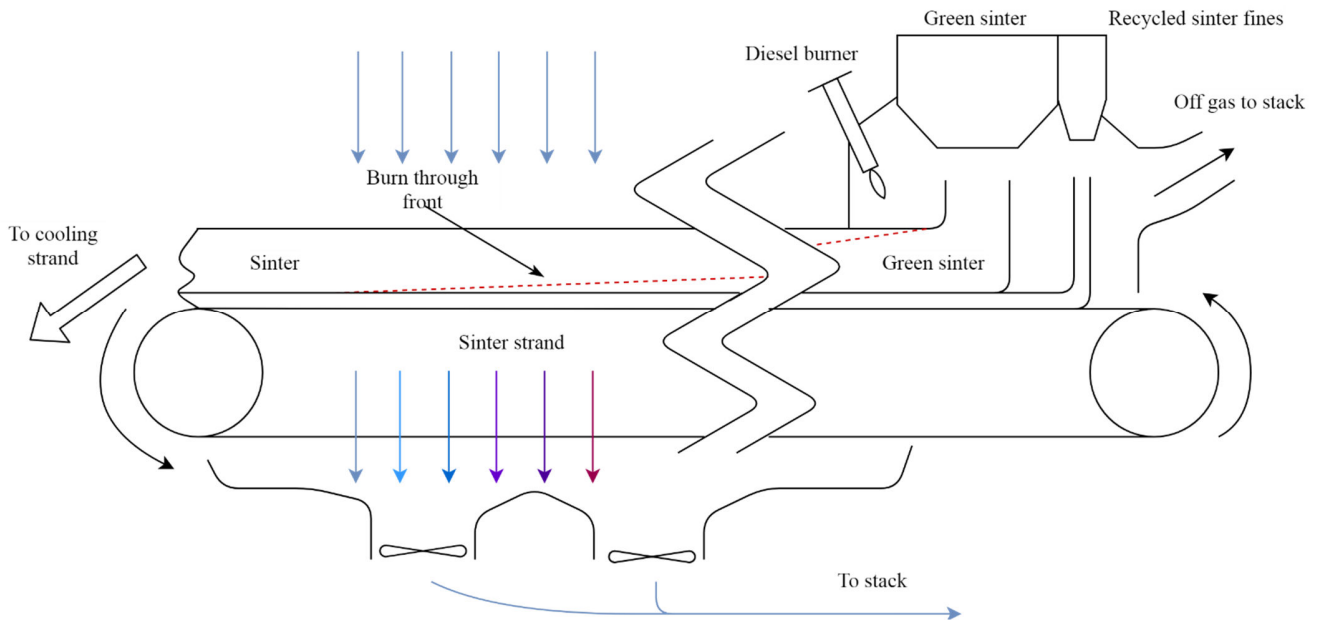

Fig. 3: Direct normal irradiation map of South Africa [2]

---

[1] PREMA: Energy efficient, primary production of manganese ferroalloys through the application of novel energy systems in the drying and pre-heating of furnace feed materials;

Fig. 4: Schematic of the sinter plant operation [4].

1.2.2 The sinter plant

The Kalagadi sinter plant was built to locally beneficiate the mined manganese ore prior to transport. In the beneficiation process the Mn content is increased from 38 % to approximately 47 % [3]. The production capacity of the sinter plant is up to 9000 t of sinter per day [4]. Fig. 4 illustrates a schematic of the sinter plant.

The green sinter (crushed ore blended with 10 % coke) is loaded onto a conveyor belt. There, the green sinter is exposed to the heat of a diesel burner in the ignition hood. The hot air is sucked through the sinter and the conveyor belt to heat the ore. The coke content in the green sinter ignites when reaching approximately 600 °C. The additional heat provided by the coke combustion increases the temperature to approximately 1200 °C for the sintering process [4].

This self-combustion is initiated in the ignition hood. From there, as the conveyor moves sinter and the ignited top layer further along, fresh air continues to be sucked through the sinter and belt. This maintains the sinter process which eventually burns through the entire layer of sinter.

As illustrated in Fig. 4, a bottom layer of recycled sinter fines is used to separate the hot burn front from the conveyor belt. Towards the end of the conveyor belt the sinter process is concluded and the sinter is offloaded for cooling and shipping. The sinter process off-gas of about 200 °C is used to pre-heat the sinter prior to loading it into the ignition hood [4]. The current diesel consumption in the sinter process is 2.56 kg per ton of produced sinter or up to 23 040 kg per day, equivalating to about 276 MWh$_t$ [4].

2. CST technology and modelling

A concentrating solar thermal (CST) plant is modelled to estimate the levelized cost of heat (LCOH) to permit comparing these to the cost of heat provided by combusting diesel. The CST plant considered uses the DLR's CentRec particle receiver technology, capable of achieving temperatures in excess of 1000 °C. The concentrator is Stellenbosch University's HelioPod technology, a heliostat shown to have excellent optical performance while suggesting low cost of manufacturing and deployment.

The CST plant is modelled considering the 1 m^2 aperture/2.5 MW$_t$ existing CentRec prototype and the existing HelioPod technology. Projections towards LCOH reduction through improvements are provided in the following sections.

2.1 Plant configuration

The moderate costs associated with the particles (see section 2.3) combined with an energy density of 200 kWh/t or 400 kWh/m^3 (heat extraction cooling the particles from 900 °C to return at 200 °C in the heat exchanger) permits cost effective utilization of the particles as direct storage medium. A benefit of such a solution is that storage containers can be moved by trucks and that a CST plant can be more easily integrated into an existing process. Firstly, the CST plant can be spatially removed from a process generating air pollution to protect mirror cleanliness. Secondly, the integration into the process requires less space and not a CST plant directly adjacent to the factory (see Fig. 5) [5].

Consequently, the solar field can be strategically positioned at available land and predominant wind directions can be taken into

account. On factory side the integration is minimized to buffer storage and heat exchanger.
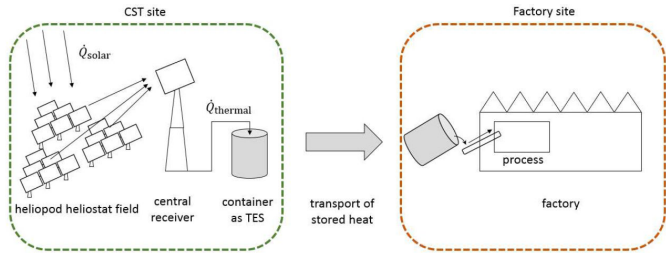

Fig. 5: Spatial separation of CST plant and process as introduced by [5]

2.2 Heliostat

2.2.1 HelioPod technology

The Solar Thermal Energy Research Group (STERG) at Stellenbosch University developed the HelioPod heliostat technology through a Technology Innovation Agency (TIA) funded innovation initiative [6]. The HelioPod is distinguished from other conventional heliostats by six heliostats sharing a common mounting structure (see Fig. 6). Such a system is referred to as a HelioPod.

Benefit of the HelioPod design is that the need for costly ground works for heliostat foundations falls away. This advantage is further exploited by omitting trenching for cabling by replacing them with wireless communication and a PV/battery powered heliostats. The heliostats, or rather the HelioPods, are fully autonomous which permits rapid integration in the field.

A consequence of the HelioPod being fully autonomous and not mounted on a concrete foundation is the added benefit that a HelioPod may be re-deployed. With the costly assets no longer being bound to a location, this reduces the risk of an ESCO (energy service company) concept, where the CST plant owner sells heat to the process, rather than the process plant operating and owning a CST plant.

While the pod structure of the HelioPod removes the need for costly ground preparation, the HelioPod cost predictions are excellent when compared to current heliostat costs. The cost of the demonstration technology was estimated at 144 $/m^2 while increased production rates and learning rates are expected to drive down costs to around 85 $/m^2 within a short while after roll-out [7]. This places the HelioPod on a trajectory towards the SunShot goals of heliostat costs of 50 $/m^2 by 2030 [8] assuming further innovation outside economies of scale and learning rates.

Besides the listed cost and deployment benefits contained in the HelioPod technology, the system showed excellent optical performance.

Fig. 6: Photograph of a HelioPod while tracking

Some of the specifications of the HelioPod are listed in Table 1. The facet focal length is variable depending on an optimization for a required plant/large scale roll out. For the purpose of this analysis it is assumed that eight different focal lengths are deployed in the heliostat field.

specification	value	unit
number of heliostats per HelioPod	6	-
facet optical aperture	1.830 x 1.220	m
facet focal length	variable	-
tracking mechanism	fixed-horizontal	-
drives	2x linear actuator	-
foundation	none	
surface slope error + shape error	< 1.0	mrad
pointing error	0.5	mrad

Table 1: HelioPod specifications

2.2.2 Heliostat field model

The heliostat field performance was modelled using a densely packed circular field layout. The solar field size was established by adapting the field size for noon, spring equinox at the given site, until 2.5 MW$_t$ receiver output were achieved.

Table 4 summarizes the heliostat field performance. The heliostat field layout was densely-packed staggered arrangement of HelioPods. The field is entirely south of the receiver and optimization work of the HelioPod positions has not been conducted, providing room for improved performance. The field is illustrated in Fig. 7.

A ray-tracing software (Tonatiuh) was then used to establish the heliostat field's optical efficiency. For that purpose the heliostat field optical efficiency was recorded in hourly resolution for
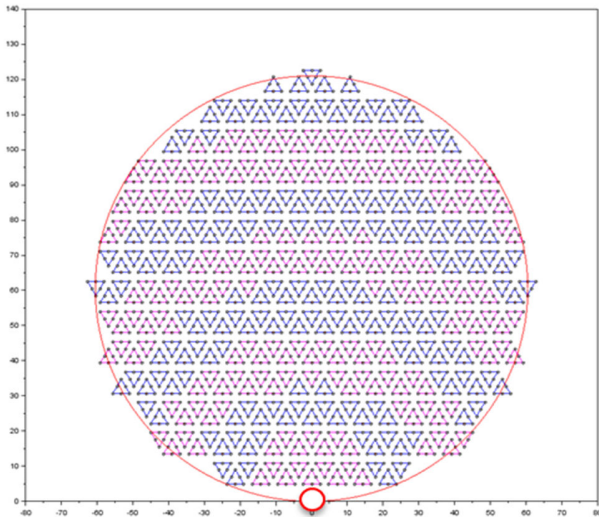
Fig. 7: Circular densely packed heliostat field layout. The changing colour of the HelioPods indicates different facet canting radii, eight in total. The central receiver location is provided at bottom centre.

summer solstice, winter solstice and spring/autumn equinox. An efficiency map was then generated permitting interpolation of heliostat field performance for any given sun position during a year.

2.3 Receiver

The CentRec receiver is modelled based on the $1 \text{ m}^2/2.5 \text{ MW}_t$ dimension investigated in [5]. The CentRec receiver is a novel particle receiver technology where small particles are directly irradiated by concentrated solar irradiation and heated to high temperatures in the process. The receiver is introduced below, followed by insight into performance data of an ongoing test campaign in Jülich, Germany.

2.3.1 Technology

The benefit of particle receivers is seen in the direct irradiation of particles by solar irradiation, therewith removing the thermal barrier of metallic tubes separating heat transfer fluid and radiation. This permits higher solar flux, higher operating temperatures and most importantly, lower costs. The CentRec receiver is a cavity receiver where a rotating absorber chamber is irradiated through the aperture as illustrated in Fig. 8. Cold particles are introduced into the receiver from above and, due to rotation of the receiver, form a film on the receiver wall.

Through adjustment of the receiver's rotating velocity a stable, thin and optically closed particle film can be maintained for a wide range of particle flow rates. The heliostat field concentrates the sun light onto the receiver aperture and directly heats the particles. The hot particles are collected through a collection ring and moved to a storage facilty.
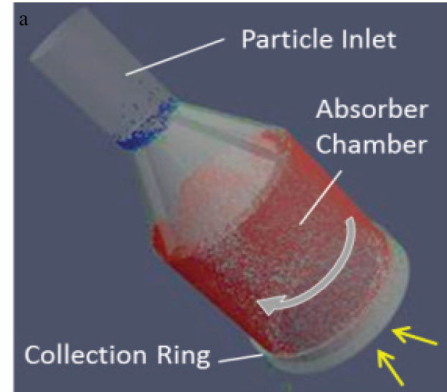

Fig. 8: The CentRec receiver operating principle [9].

For the purpose of this paper the receiver model was simplified to a solar-thermal efficiency of 90 %, which corresponds well with performance data provided in [5].

2.3.2 Prototype tests at the Solar Tower Jülich

A CentRec prototype receiver test system was installed at the Solar Tower Jülich, Germany, in 2017 as can be seen in Fig. 9. It allows the validation of the CentRec® receiver under real conditions in an overall test setup. Specifications of the prototype are given in Table 2.

Up to now, a very promising start-up of the CentRec® system has been reached in very short time. Temperatures of up to 775 °C have been achieved at the stationary receiver outlet with even higher temperatures > 900 °C inside the receiver (see Fig. 11) [10]. A homogenous particle film and a robust operation have been observed allowing high solar fluxes and transients. Especially the homogenous particle temperature distribution on the circumference of the receiver shows that the receiver principle works well.

Fig. 9: The CentRec 1 m^2 prototype receiver during installation in Jülich [10]

Fig. 10: Receiver in operation [10]

Fig. 11: Thermal camera imaging of the receiver and particle temperature [10]

The still large temperature difference between the maximum particle temperature of > 900 °C in the receiver and the particle temperature at the stationary outlet of 775 °C is due to a partly damaged insulation in the stationary collection ring and the operation of the receiver in very low part-load, just at the limit of reaching the design temperature.

aperture area and diameter		1 m², 1.13 m
rotation axis inclination		45°
thermal power	validation test setup	500 kW$_t$
	commercial setup	2,500 kW$_t$
receiver outlet temperature	minimum	900°C
	design	1,000°C
particle mass flow at 2.5 MW$_t$, 200 °C/ 900 °C receiver inlet/outlet temperature		3 kg/s
rotational speed		approx. 45 rpm
installed rotational drive motor capacity		7,5 kW$_e$

Table 2: Specifications of CentRec prototype [10]

As the heliostat field at the Solar Tower Jülich is not designed for small, high flux density receivers on the test platform at 26 m height, tests can only be conducted up to 500 kW/m² flux density in the aperture and very high spillage can be observed during operation (see Fig. 10). Additionally, sun elevation in October was already low. Due to these restrictions, high temperatures could only be achieved by reducing the mass flow significantly.

A second test campaign is under way since April 2018 with the focus on reaching even higher temperatures and the generation of stationary measurements for receiver model validation.
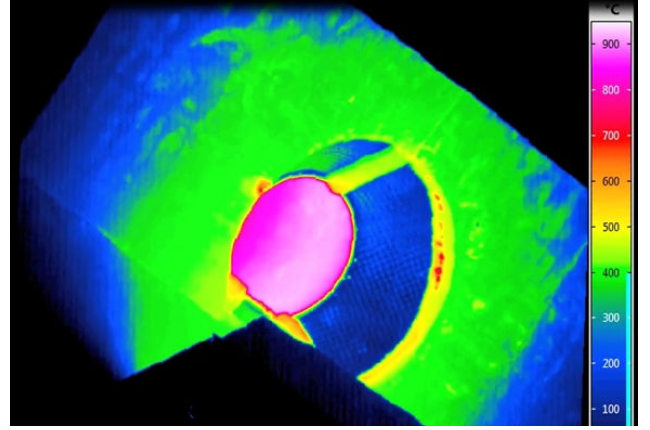
2.4 Operating strategy

The modelled central receiver system is providing 2.5 MW$_t$ peak output. The system, without being optimized for LCOH, is modelled with 12 h of thermal storage capacity and assumes to be prodiving 1 MW$_t$ output to the process whenever sufficient heat is available from the receiver and/or thermal storage. A process with higher heat requirements would see multiple tower systems.

A plant using multiple towers is expected to benefit from cost reduction in improved exploitation of mutual horizontal transport infrastructure.

2.5 Cost assumptions

The cost assumptions used to predict the LCOH are provided in Table 3. The levelized cost of heat is calculated as

$$LCOH = \frac{CRF \times CAPEX + O\&M}{\sum \dot{Q}_{t,out}}$$

where $\sum \dot{Q}_{t,out}$ is the sum of all annual heat supplied to the process, $CAPEX$ being the total capital expenditure and $O\&M$ the annual operation and maintenance cost. CRF is the capital recovery factor, calculated as

$$CRF = \frac{k_d(1 + k_d)^n}{(1 + k_d)^n - 1} + k_{ins}$$

where n is the expected plant life time, k_d the debt interest rate and k_{ins} the insurance rate.

3. Results

3.1 Performance prediction

The CST plant was modelled in hourly steady-state conditions for a representative year. A solar data set for the site was

item	value	unit
heliostat -- current	140	$/m^2
heliostat -- near term	112.5	$/m^2
heliostat -- roll-out	85	$/m^2
receiver system*	123 000	$/m^2
heat exchanger* (particle-air)	123	$/kW_t$
thermal energy storage*	14.8	$/kWh_t$
vertical particle transport*	125 460	$ per tower
horizontal transport* (truck, crane & buffer tank)	221.4	$ per installation
tower*	$7380 + 1.54*h_{tower}^{2.75}$	$ per tower
indirect cost*	22	% of capex
O&M*	3.9	% of capex
insurance*, k_{ins}	1.0	% of capex
debt interest rate, k_d	7.0	% of capex

* based on [5]

Table 3: Cost assumptions

obtained from Meteonorm (version 7.2). Further model specific information is provided in Table 4.

The model was considered for the three heliostat cost scenarios (current, near-term and roll-out). The cost break-down and LCOH result for each case is provided in Table 5.

The levelized cost of heat provided by the CST plant is predicted to range from 389 R/MWh$_t$ to 474 R/MWh$_t$. The sensitivity of approximately 20 % to changes in the heliostat cost assumption is due to the heliostat field being the single biggest cost component of the CST plant at 34 % to 45 % of the plant's capital cost.

Of interest is the comparison between the LCOH from the CST plant and the cost of burning diesel fuel. Since the actual purchase cost of diesel fuel for the sintering plant is unknown, a band between the possible cost ranges is considered here. The bottom range is combusting diesel at the cost of Brent crude oil. At the current cost of 75 $/barrel this translates to 563 R/MWh$_t$. A recently stable rise of the global oil price (Fig. 12) suggests this rate to increase further in future. Such stable oil price development is however preceded by a decade of high fluctuations between just above 30 $/bbl and almost 150 $/bbl. It is interesting to note that all three LCOH provide heat at rates below combusting diesel at current Brent crude oil price.

The other end of the band assumes the cost based on diesel fuel available at petrol stations. A diesel price of currently 13.6 R/l contains RAF and fuel levy. For mining operations 80 % of RAF at 1.93 R/l and 80 % of fuel levy at 1.288 R/l are refundable [11]. Deducting these refunds gives a cost of heat at about 1107 R/MWh$_t$ for combusting diesel. Likely, the cost of diesel at

	specification	value	unit
site data	site latitude	-27.221591	°N
	site longitude	22.898324	°E
	site DNI	2752	kWh/(m^2 a)
optical data	tower height	40	m
	receiver tilt angle	45	°
	solar field size	4956	m^2
	average solar field efficiency	49	%
receiver/TES	receiver aperture	1	m^2
	TES capacity	12	h
production	production	5898	MWh$_t$/a
	capacity factor	67	%

Table 4: CST model summary

bulk supply rates is in fact below this figure but transport costs to the Northern Cape are also not included.

Due to insufficient information about actual fuel costs, R900 R/MWh$_t$ are assumed for an economic assessment. Assuming the LCOH case with the mature heliostat cost of 85 $/m^2 the pay-back period of a CST plant would be 5.9 years. An ESCO with 7 % weighed capital costs could offer heat at only 43 % of the actual costs or achieve significantly higher returns at higher heat selling prices to reflect the risks for the ESCO associated with the build-up of a new market.

item	unit	immature	medium	mature
cost heliostat	k$	693.8	557.6	421.3
cost receiver	k$		123.0	
cost heat exchanger	k$		123.0	
cost horizontal transport	k$		177.1	
cost thermal energy storage	k$		125.5	
cost vertical transport	k$		221.4	
cost tower	k$		46.5	
capex	k$	1510.3	1374.0	1237.7
indirect cost	k$	332.3	302.3	272.3
total invest	k$	1842.6	1676.3	1510.1
O&M cost	k$/a	58.9	53.6	48.3
plant lifetime	a		25.0	
insurance cost	-		0.01	
debt interest rate	-		0.07	
LCOH	$/MWht	39.9	36.3	32.7
LCOH	R/MWh$_t$	474.2	431.4	388.6

Table 5: Plant costs and LCOH

Fig. 12: Price development of Brent crude oil since 2016

For comparison the current rate of marine diesel is also considered at 660 $/t or 655 R/MWh$_t$, excluding cost of delivery to the Northern Cape province [12].

3.2 improvement potential

The LCOH levels have potential for further improvement. The CentRec central receiver system is suggested to become more cost effective with increased receiver dimensions. Upscaling from the current 1 m^2 to larger aperture diameter to the range of 20 m^2 is suggested to result in significantly improved project economics while being technically feasible.

The HelioPod technology is projected to reach 85 $/m^2 in the near future, considering a technology roll-out and associated economies of scale as well as learning rates. With further innovation of the technology or alternative concepts a look at the SunShot goal of 50 $/m^2 is of interest. Considering such costs for the heliostat field the LCOH drops further to 334 R/MWh$_t$.

Fig. 13 compares the LCOH of CST to several fuel cost assumptions. The two lines for brent crude are representing current cost of 75 $/bbl and for reference 100 $/bbl.
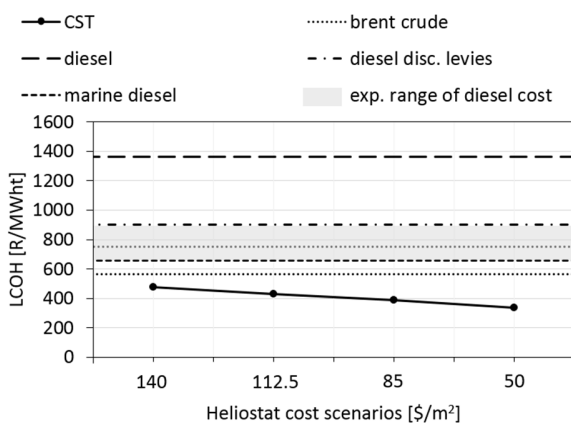

Fig. 13: LCOH of CST compared to various fuel costs

4. Discussion

The high-level analysis to establish the viability of implementing

CST in a Mn sinter plant showed that the technology has the potential to provide heat at costs significantly below current diesel rates. In fact, the cost of CST-generated heat is expected to be below the cost of Brent crude oil.

A more detailed analysis is recommended to establish technical opportunities of integrating CST heating unit into the existing sinter plant and to further investigate the potential to displace diesel fuel. With its excellent solar resource, South Africa is well positioned to be a potential supplier of future global markets with carbon neutral hydrogen generated from CSP/PV plants. Such fuels in combination with the analysed CST plant lead to the potential of fully displacing the current diesel fuel.

Significant cost reduction for heat generation is expected for technology maturity and large scale roll-out. Further cost reductions expected for the CSP industry will also translate to reducing the production cost of CST plants.

Acknowledgements

References

[1]   European Commission, "2050 Energy strategy," Luxembourg, 2012.

[2]   The World Bank, "Solar resource data: SolarGIS," 2017. [Online]. Available: https://solargis.com/maps-and-gis-data/download/south-africa. [Accessed: 20-Mar-2018].

[3]   Kalagadi Manganese, "Kalagadi Manganese website," 2018. [Online]. Available: http://www.kalahariresources.co.za. [Accessed: 11-Jan-2018].

[4]   S. Hockaday, M. Lubkoll, F. Dinter, and T. M. Harms, "Introducing solar thermal heat into minerals processing: A case study on replacing a diesel burner at a sinter plant," in *SASEC2018 (submitted)*, 2018.

[5]   L. Amsbeck, B. Behrendt, T. Prosin, and R. Buck, "Particle tower system with direct absorption centrifugal receiver for high temperature process heat," *Energy Procedia*, pp. 0–6, 2015.

[6]   P. Gauché, "Helio100," 2016. [Online]. Available: http://helio100.sun.ac.za/. [Accessed: 16-Aug-2015].

[7]   J. N. Larmuth, W. A. Landman, and P. Gauché, "A top-down approach to heliostat cost reduction," *AIP Conf. Proc.*, vol. 020013, no. 1734, pp. 0–8, 2016.

[8]   SETO, "SunShot 2030," 2017. [Online]. Available: https://www.energy.gov/eere/solar/sunshot-2030. [Accessed: 01-Apr-2018].

[9]   L. Amsbeck, R. Buck, T. Rehbock, T. Prosin, and P. Schwarzbözl, "Solar sludge drying demonstration plant," in *"SYMPHOS 2017", 4th International Symposium on Innovation and Technology in the Phosphate Industry*, 2017, vol. 00, pp. 0–7.

[10]   L. Amsbeck, R. Buck, J. Rheinländer, B. Schlögl-Knothe, S. Schmitz, M. Sibum, H. Stadler, and R. Uhlig, "First on-sun tests of a centrifugal particle receiver system," in *Proceedings of the ASME 2018 Power and Energy Conference*.

[11]   SARS, *Schedule 6 - Rebates and refunds of excise duties, fuel levy, road accident fund levy, environmental levy and health promotion levy*. Pretoria: SARS, 2018.

[12]   BIX, "Bunker Index MDO," 2018. [Online]. Available: http://www.bunkerindex.com/prices/bixfree.php?priceindex_id=4. [Accessed: 08-May-2018].